Memoirs of the Faculty of Engineering, Nagoya University
Vol. 39, No. 1 (1987) —Research Report—

IMPROVEMENTS ON ACCURACY AND EFFICIENCY FOR CALCULATION OF TRANSONIC VISCOUS FLOW AROUND AN AIRFOIL

YI-YUN WANG and TOSHI FUJIWARA

Department of Aeronautical Engineering

(Received May 30, 1987)

Abstract

The use of the implicit Beam-Warming scheme is restricted due to its high cost. A LU-decomposition is utilized to avoid inverting block tridiagonal matrices. The use of local time step to reach a steady solution remarkably accelerates convergence rate. A mixed nonlinear dissipation is used to enhance shock resolution. The boundary treatments of like-characteristics improve accuracy and reliability. Only 3 minutes are necessary for one case on FUJITSU VP-100 supercomputer.

1. Background

The two-dimensional full Navier-Stokes equations have been solved[1,2]. The purpose of retaining all viscous terms is that a higher accuracy is expected. However, the difference between the results calculated by two-(only one viscous term in η-direction is retained) and three-level scheme is not conspicuous. It will become smaller at a high Reynolds number because computational grids are highly concentrated near body surface and, as a result, mesh aspect ratio becomes very large. All the viscous terms associated with strain rates along body surface are comparatively small and negligible. Thereafter, we will consider the governing equations only under the 'thin-layer' assumption, that is

$$\hat{U}_\tau+\hat{E}_\xi+\hat{F}_\eta=\hat{S}_\eta/Re, \tag{1}$$

where

$$\hat{S}=J^{-1}\begin{pmatrix} 0 \\ \mu(\eta_x^2+\eta_y^2)u_\eta+(\mu/3)(\eta_x u_\eta+\eta_y v_\eta)\eta_x \\ \mu(\eta_x^2+\eta_y^2)v_\eta+(\mu/3)(\eta_x u_\eta+\eta_y v_\eta)\eta_y \\ \{(\eta_x^2+\eta_y^2)[0.5\mu(u^2+v^2)_\eta+xPr^{-1}(\gamma-1)^{-1}(a^2)_\eta]+ \\ +(\mu/3)(\eta_x u+\eta_y v)(\eta_x u_\eta+\eta_y v_\eta)\} \end{pmatrix}. \tag{2}$$

A corresponding factorization implicit method adapted from Beam and Warming is given by

$$(1+\Delta\tau\delta_\xi\hat{A}^n-\varepsilon_I J^{-1}\nabla_\xi\Delta_\xi J)(1+\Delta\tau\delta_\eta\hat{B}^n-\Delta\tau Re^{-1}\delta_\eta\hat{M}^n-\varepsilon_I J^{-1}\nabla_\eta\Delta_\eta J)\Delta\hat{U}^n$$
$$=-\Delta\tau(\delta_\xi\hat{E}+\delta_\eta\hat{F}-Re^{-1}\delta_\eta\hat{S})^n-\varepsilon_E J^{-1}[(\nabla_\xi\Delta_\xi)^2+(\nabla_\eta\Delta_\eta)^2]J\hat{U}^n, \tag{3}$$

where $\hat{A}$, $\hat{B}$ and $\hat{M}$ are the Jacobian matrices $\partial\hat{E}/\partial\hat{U}$, $\partial\hat{F}/\partial\hat{U}$ and $\partial\hat{S}/\partial\hat{U}$. The notations δ, ∇ and Δ denote central, backward and forward difference, respectively. Since in general $\Delta\xi=\Delta\eta=1$, they have been omitted. Using central difference operators, the procedure implicitly solving the left-hand-side factors results in the inversion of a block 4×4 tridiagonal matrix. That takes 60% of the total computational expense for an inviscid flow. It is less for a viscous flow because this cost remains fixed while calculation of viscous terms, i. e. the viscous Jacobians and turbulence model terms increases the overall count. How to save the computing cost became a subject sought by many authors of late years. In order to gain a steady flow, which is determined only by the right-hand side of Eq. (3) so long as the procedure is convergent, changing the form of left-hand-side factors is permitted. One of the approaches proved to be useful is the reduction of block size, shown for instance in Ref. 3. Another approach used more widely is diagonalization[4].

The flux Jacobians $\hat{A}$ and $\hat{B}$ all have real eigenvalues and a complete set of eigenvectors. Therefore, they can be diagonalized as

$$\hat{A}=T_\xi\Lambda_\xi T_\xi^{-1},\quad \hat{B}=T_\eta\Lambda_\eta T_\eta^{-1}. \tag{4}$$

Matrices T_ξ and T_η consist of the eigenvectors of $\hat{A}$ and $\hat{B}$, respectively. They are written out in Appendix A. We then rewrite Λ as follows:

$$\Lambda=\Lambda^+ +\Lambda^-, \tag{5}$$

$$\Lambda^\pm=(\Lambda\pm|\Lambda|)/2. \tag{6}$$

Substituting Eq. (6) into Eq. (3), we obtain the following equations for an inviscid flow:

$$T_\xi[I+\Delta\tau\delta_\xi(\Lambda_\xi^+ +\Lambda_\xi^-)-\varepsilon_I J^{-1}\nabla_\xi\Delta_\xi J]T_\xi^{-1}T_\eta[I+\Delta\tau\delta_\eta(\Lambda_\eta^+ +\Lambda_\eta^-)$$
$$-\varepsilon_I J^{-1}\nabla_\eta\Delta_\eta J]T_\eta^{-1}\Delta\hat{U}^n=\text{RHS of Eq. (3)}. \tag{7}$$

Because the elements of $\Lambda^\pm$ possess the same sign, it enables us to use the upwind scheme. The difference operators of the left-hand side now have been diagonalized and block tridiagonal inversion is reduced to scalar tridiagonal one. Thus, the

computational expense is greatly decreased.

For a viscous flow, the block tridiagonal inversion in η-direction is still necessary because the diagonalization of $\hat{M}$ is impossible. In addition, scalar pentadiagonal inversion is needed when using three-point upwind differencing; it is inconvenient. The following LU-ADI solver would have more convenience in the above two respects.

2. LU-ADI Solver[5)]

As is well known, a convective model equation with speed c

$$\frac{\partial u}{\partial t}+c\frac{\partial u}{\partial x}=0, \tag{8}$$

has the stability condition

$$c\frac{\Delta t}{\Delta x}\leqslant 1, \tag{9}$$

when an explicit scheme is used. On the other hand, a diffusive model equation with kinematic viscosity $\tilde{\nu}$

$$\frac{\partial u}{\partial t}=\tilde{\nu}\frac{\partial^2 u}{\partial x^2}, \tag{10}$$

has the stability condition

$$2\tilde{\nu}\frac{\Delta t}{\Delta x^2}\leqslant 1. \tag{11}$$

A mixed model equation

$$\frac{\partial u}{\partial t}+c\frac{\partial u}{\partial x}=\tilde{\nu}\frac{\partial^2 u}{\partial x^2}, \tag{12}$$

has the stability condition related with the above two schemes; the time step satisfies the following condition:

$$c\frac{\Delta t}{\Delta x}+2\tilde{\nu}\frac{\Delta t}{\Delta x^2}\leqslant 1 \tag{13}$$

or

$$\Delta t\leqslant\frac{\Delta x}{c+(2\tilde{\nu}/\Delta x)}. \tag{14}$$

We now return to the Navier-Stokes equations (1) and investigate momentum diffusion along body surface direction $(\eta_y,-\eta_x)$;

$$\eta_y\frac{\partial(J^{-1}\rho u)}{\partial\tau}-\eta_x\frac{\partial(J^{-1}\rho v)}{\partial\tau}$$

$$=\eta_y\frac{\partial\{Re^{-1}J^{-1}[\mu(\eta_x^2+\eta_y^2)u_\eta+(\mu/3)(\eta_x u_\eta+\eta_y v_\eta)\eta_x]\}}{\partial\eta}$$

$$-\eta_x\frac{\partial\{Re^{-1}J^{-1}[\mu(\eta_x^2+\eta_y^2)v_\eta+(\mu/3)(\eta_x u_\eta+\eta_y v_\eta)\eta_y]\}}{\partial\eta}. \tag{15}$$

Locally using linearization technique which allows all variables (except u and v) to be moved into or out of the differential notations with respect to τ or η, we obtain

$$J^{-1}\rho\frac{\partial(\eta_y u-\eta_x v)}{\partial\tau}=Re^{-1}J^{-1}\mu(\eta_x^2+\eta_y^2)\frac{\partial^2(\eta_y u-\eta_x v)}{\partial\eta^2}$$

or

$$\frac{\partial R}{\partial\tau}=\rho^{-1}Re^{-1}\mu(\eta_x^2+\eta_y^2)\frac{\partial^2 R}{\partial\eta^2}, \tag{16}$$

where

$$R=\eta_y u-\eta_x v \tag{17}$$

is the strain velocity in ξ-direction. Comparing with Eq. (10), we have

$$\tilde{\nu}=\rho^{-1}Re^{-1}\mu(\eta_x^2+\eta_y^2), \tag{18}$$

and the stability condition (14) becomes

$$\Delta\tau\leqslant\frac{\Delta\eta}{\lambda^+ +\nu}, \tag{19}$$

where λ^+ is an element of matrix Λ^+ and

$$\nu=2\mu(\eta_x^2+\eta_y^2)/(\rho Re\Delta\eta). \tag{20}$$

In order to maintain the stability of the thin-layer viscous terms, we approximately replace viscous effect $\delta_\eta\hat{M}$ in the left-hand side of Eq. (3) by Eq. (20). Thus, the diagonalized Eq. (7) is still applicable even to a viscous flow, while only Eq. (6) as used for $\hat{B}$ would be modified as follows:

$$\Lambda_\eta^\pm=(\Lambda_\eta\pm|\Lambda_\eta|)/2\pm\nu I. \tag{21}$$

The fourth-order central differencing is used for the convective terms in the right-hand side to improve accuracy for an inviscid flow field, and the first-order three-point upwind differencing is used so as to be consistent with the fourth-order one; therefore, a second-order truncation error is produced as a useful artificial dissipative term. Both the fourth-order central differencing and the first-order upwind one are expressed in the following:

$$\delta_\xi\hat{E}_i=(-\hat{E}_{i+2}+8\hat{E}_{i+1}-8\hat{E}_{i-1}+\hat{E}_{i-2})/(12\Delta\xi)+O(\Delta\xi^4), \tag{22}$$

$$\nabla_\xi\Lambda^+_{\xi,i}=(\Lambda^+_{\xi,i-2}-8\Lambda^+_{\xi,i-1}+7\Lambda^+_{\xi,i})/(6\Delta\xi)+O(\Delta\xi), \tag{23}$$

$$\Delta_\xi\Lambda^-_{\xi,i}=(-7\Lambda^-_{\xi,i}+8\Lambda^-_{\xi,i+1}-\Lambda^-_{\xi,i+2})/(6\Delta\xi)+O(\Delta\xi). \tag{24}$$

Then we have

$$I+\Delta\tau(\nabla_\xi A^+_{\xi,i}+\Delta_\xi A^-_{\xi,i})=L_A+M_A+N_A, \tag{25}$$

where

$$L_A=\Delta\tau(A^+_{\xi,i-2}-8A^+_{\xi,i-1})/(6\Delta\xi), \tag{26}$$

$$M_A=I+\Delta\tau(A^+_{\xi,i}-A^-_{\xi,i})7/(6\Delta\xi), \tag{27}$$

$$N_A=\Delta\tau(-A^-_{\xi,i+2}+8A^-_{\xi,i+1})/(6\Delta\xi). \tag{28}$$

Since $M_A=O(1)$, L_A, N_A are $O(\Delta\tau)$, and the product of L_A and N_A is negligible, a scalar pentadiagonal matrix shown in Eq. (25) is decomposed into the product of the upper and lower scalar tridiagonal ones, L_A+M_A and M_A^{-1} (M_A+N_A). As a result, the inversion procedure becomes quite easy.

Before concluding this section, we supplement to analyze the stability of the Beam-Warming scheme for the model equation (8) and explain why selecting three-point upwind differencing.

a) If three-point central differencing is adopted in both the left- and right-hand sides, we have

$$\Delta u^n_i+\left(c\frac{\Delta t}{\Delta x}\right)\frac{\Delta u^n_{i+1}-\Delta u^n_{i-1}}{2}=-\left(c\frac{\Delta t}{\Delta x}\right)\frac{u^n_{i+1}-u^n_{i-1}}{2} \tag{29}$$

or

$$(G-1)[1+(\sigma/2)(e^{Ik\Delta x}-e^{-Ik\Delta x})]=-(\sigma/2)(e^{Ik\Delta x}-e^{-Ik\Delta x}), \tag{30}$$

$$G=1/[1+I\cdot\sin k\Delta x\cdot H], \tag{31}$$

where $\sigma=c\Delta t/\Delta x$ and then

$$H_1=\sigma. \tag{32}$$

b) If two-point upwind differencing is used in the left-hand side, Eq. (29) becomes

$$\Delta u^n_i+\sigma(\Delta u^n_i-\Delta u^n_{i-1})=-(\sigma/2)(u^n_{i+1}-u^n_{i-1}). \tag{33}$$

We obtain the amplification factor G possessing a form identical with Eq. (31), and

$$H_2=\frac{\sigma}{1+\sigma(1-\cos k\Delta x)}. \tag{34}$$

It is easy to find that $H_2\leqslant H_1$, i. e. this scheme has a stability less than central one.

c) If three-point upwind differencing is used in the left-hand side and, correspondingly, fourth-order one is applied in the right-hand side, we obtain

$$\Delta u^n_i+(\sigma/6)(7\Delta u^n_i-8\Delta u^n_{i-1}+\Delta u^n_{i-2})$$
$$=-(\sigma/12)(-u^n_{i+2}+8u^n_{i+1}-8u^n_{i-1}+u^n_{i-2}) \tag{35}$$

and

$$H_3=\frac{(\sigma/3)(4-\cos k\Delta x)}{1+(\sigma/3)(1-\cos k\Delta x)(3-\cos k\Delta x)}. \tag{36}$$

$|G|$ reduces to 1 when $\sin k\Delta x=0$. Assuming $\sin k\Delta x=1$, that is to say, $\cos k\Delta x=0$, we have $H_2=\sigma/(1+\sigma)$ whereas $H_3=(4\sigma/3)/(1+\sigma)$. It shows that the use of three-point upwind differencing has better stability than two-point scheme, although it is still less than central one.

For further improving the stability, we use the three-level scheme also in time direction ($\delta=1/2$), as in Ref. 1. It does not add any difficulty and may receive better effect.

3. Local Time Steps

Several ways of space-varying time steps have been proposed to cope with the contradiction that an extremely small time step is required in a boundary layer while a moderate one is required for an outer flow which is basically inviscid. Although the flow field is not simultaneous before converging to a steady solution, it is permitted when we are interested only in a steady solution.

One form of the variable time step size is

$$\Delta\tau=\frac{\Delta\tau|_{ref}}{|\hat{u}|+a\sqrt{\hat{\xi}_x^2+\hat{\xi}_y^2}+|\hat{v}|+a\sqrt{\eta_x^2+\eta_y^2}}, \tag{37}$$

which is approximately a constant CFL condition. Another widely used one is

$$\Delta\tau=\frac{\Delta\tau|_{ref}}{1+\sqrt{J}}, \tag{38}$$

which is a purely geometric variation only dependent on grids. Both of them are successful in our calculations. But the latter one seems more simple and convenient.

The parameter $\Delta\tau|_{ref}$ is initially set to $O(1)$, which corresponds to the Courant number about $O(1)$, in order to suppress the starting transient. After that, we gradually amplify $\Delta\tau|_{ref}$ to accelerate convergence and correspondingly to reduce the evaluated error per unit time scale.

4. Combination of Second-and Fourth-Order Dissipations

The approach of adding a constant coefficient fourth-order explicit dissipation has been used in Ref. 1 and proved effective to obtain a convergent solution, although it generates overshoot in front of a shock wave. Severe oscillations are sometimes produced on refined meshes, even causing numerical instability. This is an inherent disadvantage of fourth-order dissipation as analyzed in Ref. 6. Consider the model equation (8) with the initial condition

$$u_i^n=\begin{cases}1 & (i\leqslant I-1),\\ 0 & (i=I),\\ -1 & (i\geqslant I+1).\end{cases} \tag{39}$$

We form a propagating solution from the above initial condition using the scheme

$$u_i^{n+1}=u_i^n-(\sigma/2)\,(u_{i+1}^n-u_{i-1}^n)+f_i. \tag{40}$$

Taking Courant number $\sigma=c\Delta t/\Delta x=1$ and using the fourth-order dissipation

$$f_i^{(4)}=-(1/4)\,(u_{i+2}^n-4u_{i+1}^n+6u_i^n-4u_{i-1}^n+u_{i-2}^n), \tag{41}$$

the solution after one step becomes

$$u_i^{n+1}=\begin{cases} 1 & (i\leqslant I-3),\\ 5/4 & (i=I-2),\\ 1 & (i=I-1),\\ 1 & (i=I),\\ 0 & (i=I+1),\\ -5/4 & (i=I+2),\\ -1 & (i\geqslant I+3). \end{cases} \tag{42}$$

It shows that overshoots are induced in both sides of the discontinuity. While the second-order dissipation

$$f_i^{(2)}=(u_{i+1}^n-2u_i^n+u_{i-1}^n)/2 \tag{43}$$

produces the solution that advanced one time step

$$u_i^{n+1}=\begin{cases} 1 & (i\leqslant I),\\ 0 & (i=I+1),\\ -1 & (i\geqslant I+2), \end{cases} \tag{44}$$

which maintains the monotonousness across the discontinuity.

A combination of second- and fourth-order dissipations is proposed by Jameson and has been applied to computing viscous flows by Pulliam and Steger[4]. It can eliminate the oscillations at the shock using a slightly complicated form

$$\nabla_\xi(\sigma_{i+1,j}J_{i+1,j}^{-1}+\sigma_{i,j}J_{i,j}^{-1})\,(\varepsilon_{i,j}^{(2)}\Delta_\xi-\varepsilon_{i,j}^{(4)}\Delta_\xi\nabla_\xi\Delta_\xi)\,(J\hat{U})_{i,j}, \tag{45}$$

where

$$\varepsilon_{i,j}^{(2)}=k_2\Delta\tau f(\gamma_{i+1,j},\ \gamma_{i,j},\ \gamma_{i-1,j}), \tag{46}$$

$$\varepsilon_{i,j}^{(4)}=\mathrm{Max}(0,\ k_4\Delta\tau-\varepsilon_{i,j}^{(2)}), \tag{47}$$

$$\gamma_{i,j}=\frac{|p_{i+1,j}-2p_{i,j}+p_{i-1,j}|}{|p_{i+1,j}+2p_{i,j}+p_{i-1,j}|}. \tag{48}$$

Typical values of the constants are $k_2=1/4$ and $k_4=1/100$. The coefficient $\sigma_{i,j}$ is

a spectral radius scaling and in two dimensions is defined as

$$\sigma_{i,j}=[|\hat{u}|+a\sqrt{\xi_x^2+\xi_y^2}+|\hat{v}|+a\sqrt{\eta_x^2+\eta_y^2}]_{i,j}, \tag{49}$$

which is a sum of the spectral radii of $\hat{A}$ and $\hat{B}$.

In our computational example, we used the above smoothing model only in ξ-direction and with the modifications

$$\sigma_{i,j,\xi}=[|\hat{u}|+a\sqrt{\xi_x^2+\xi_y^2}]_{i,j}, \quad \sigma_{i,j,\eta}=[|\hat{v}|+a\sqrt{\eta_x^2+\eta_y^2}]_{i,j}. \tag{50}$$

The smoothness indicator $f(\gamma)$ is chosen as

$$f(\gamma_{i+1,j},\ \gamma_{i,j},\ \gamma_{i-1,j})=\mathrm{Max}(\gamma_{i+1,j},\ \gamma_{i,j},\ \gamma_{i-1,j}), \tag{51}$$

which acts as a switch to cut off the fourth-order dissipation near a shock. The ratio k_2/k_4 provides a criterion of shock strength. It should be smaller when applied to a supersonic flow having a stronger shock.

The implicit dissipation in the left- hand side only acts a role to ensure stability. It is not necessary to adopt a combined second-plus fourth-order forms as in the explicit side for sharpening a shock. Due to the use of implicit upwind differencing, an inherent second-order dissipation has been always added. We only need to add fourth-order one whose form is completely identical with Eq. (45) at $k_2=0$. Excellent stability has been shown in Ref. 6.

5. Boundary Condition on Free Surface

From the characteristics theory, the number of the specifiable independent conditions on a boundary should be identical with that of the characteristic velocities pointing to the interior of the computed domain. We locally regard a flow through a free surface as one-dimensional. The four characteristic velocities λ_i are v_n, v_n, v_n+a and v_n-a, where v_n is the velocity component normal to a free surface; corresponding to λ_3 and λ_4 the locally one-dimensional Riemann invariants are given as

$$R_3=v_n+\frac{2}{\gamma-1}a, \quad R_4=v_n-\frac{2}{\gamma-1}a. \tag{52}$$

For a subsonic inflow $v_n\leqslant 0$, λ_1, λ_2 and λ_4 are all negative. Three conditions can be specified. One is R_4 and the other two are chosen as v_t and $s=ln(p/\rho^\gamma)$. They are all set to the free stream values. Another condition should represent such fact that a disturbance inside the domain propagates to outside. We choose to extrapolate R_3 from the interior flow variables. On subsonic outflow $v_n>0$, only R_4 is fixed to the free stream values while R_3, v_t and s are extrapolated.

6. Far Field Circulation Correction

The circulation integrated around a lifting airfoil in a subsonic free stream is not equal to zero and is independent of integral routes; for instance, along the

airfoil surface or along the far boundary. Artificially adding a circulation correction to the free stream as a new far boundary condition would further improve the accuracy and reliability. The test shows that such a correction greatly reduces the extent that solution depends on the size of computed domain. It enables us to obtain a reasonably good approximate solution in the domain with a radius of only about 5 chord lengths.

The corrected far boundary velocities are defined as

$$u_f=u_\infty+\frac{\beta\Gamma\sin\theta}{2\pi r[1-M_\infty^2\sin^2(\theta-\alpha)]}, \tag{53}$$

$$v_f=v_\infty-\frac{\beta\Gamma\cos\theta}{2\pi r[1-M_\infty^2\sin^2(\theta-\alpha)]}, \tag{54}$$

where the circulation $\Gamma=C_L\cdot L/2$, L is the chord length, $\beta=\sqrt{1-M_\infty^2}$ and r, θ are the polar coordinates of a point where the far boundary condition is applied; the coordinate origin is placed at the quarter-chord point on the airfoil center line. The lift acts at this point according to the theory of thin airfoils. The speed of sound is determined by

$$a_f^2=(\gamma-1)[H_\infty-(u_f^2+v_f^2)/2], \tag{55}$$

which means that the enthalpy at the boundary is equal to the constant value of the free stream.

It is not difficult to derive that the circulation given by integrating Eqs. (53) and (54) along a circle with radius r is just equal to $-\Gamma$; we use a definite integral fomula

$$\int_0^\pi\frac{dx}{a+b\cos x}=\frac{\pi}{\sqrt{a^2-b^2}}\quad(a>|b|). \tag{56}$$

The factor $\beta/[1-M_\infty^2\sin^2(\theta-\alpha)]$ is a compressibility correction. Assuming the factor equal to 1, Eqs. (53) and (54) represent a uniform flow plus an incompressible point vortex flow with strength Γ.

7. Example

All of the above improvements have been used to repeat the calculation for the RAE 2822 airfoil using the same Mach number 0.75, angle of attack 3.19 degree and Reynolds number 6.2×10^6 as in Ref. 2. The used meshes are 173×49 as is identical with Ref. 7, where 133 points are distributed on airfoil surface. The computational results show satisfactory improvements in both accuracy and efficiency.

Fig. 1 shows excellent convergence. The dashed line describes the convergence history of $\overline{\Delta\rho}$ defined as

$$\overline{\Delta\rho}=\sqrt{[\textstyle\sum_{i,j}(\Delta\rho_{i,j})^2]/N}. \tag{57}$$

The parameter $\Delta\tau|_{ref}$ is first set to 4 in the expression of a varying time step, Eq. (38). After 200 steps, we amplify it at every step with a factor equivalent to twice

for every 100 steps and correspondingly reduce the evaluated $\overline{\Delta\rho}$ divided by the overall multiple that $\Delta\tau|_{ref}$ is amplified. Thus, the mean density variation of 10^{-9} of the initial magnitude is achieved only through 1200 steps and simultaneously, the total lift coefficient C_L remains unchanged in the first 3 digits as shown by the solid line in Fig. 1. The procedure has continuously advanced until the Courant number reaches about $O(10^3)$ at the end. But such technique of amplifying the time step can not be limitlessly used, because it would cause a large truncation error and destroy the condition allowing LU decomposition; that is, the product of L_A and N_A is negligible in comparison with M_A.

The computation required about 0.18 μsec per grid per step on a FUJITSU VP-100 supercomputer. The entire calculation took about 3 minutes for 173×49 meshes.

Fig. 2 shows that the use of combined second- and fourth-order dissipations eliminated overshoot in front of a shock. A monotonous solution is obtained across the shock.

Fig. 3 illustrates a set of equi-Mach-number lines with interval $\Delta M=0.04$. One drawn by a thick line corresponds to $M=1$. The maximum Mach number in flow field is about 1.35. A shock wave still occupies a wider band because of insufficient grids in this region.

A set of particle paths is shown in Fig. 4 (a). It is obtained by assuming that the particles are released from somewhere in front of the leading edge along a line perpendicular to the free stream direction and then integrating the velocity field with the lapse of time. We deliberately have left the picture unfilled in order to show a physical phenomenon that the upper flow above the boundary layer has higher velocities and lower pressures than the lower one for a lifting airfoil. While the pressure is maintained approximately constant across the boundary layer according to the boundary layer theory, such a phenomenon holds even for an entirely viscous flow. Fig. 4 (b) is a picture of particle paths, where the dashed line consists of wake points which is a trace of minimum velocity values along η-directions. Although it naturally does not possess adequate accuracy like particle paths, it can

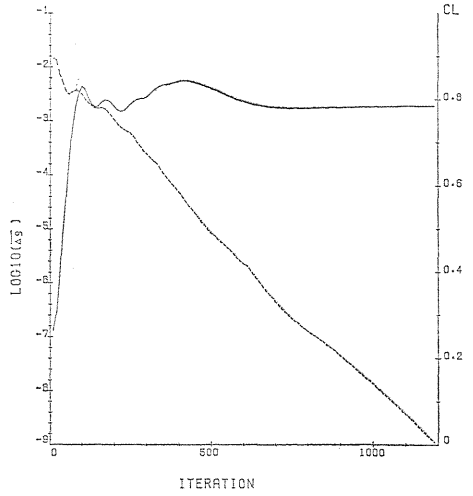

Fig. 1. Convergence history.

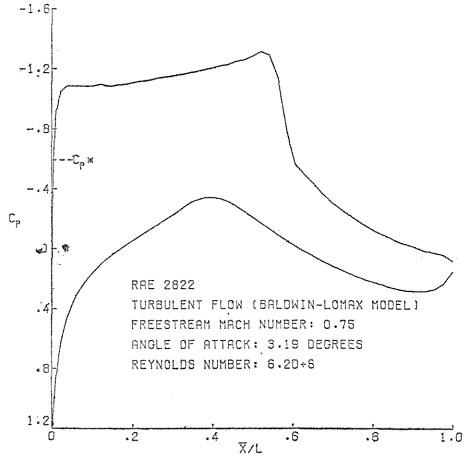

Fig. 2. Monotonous variation of pressure coefficient across the shock.

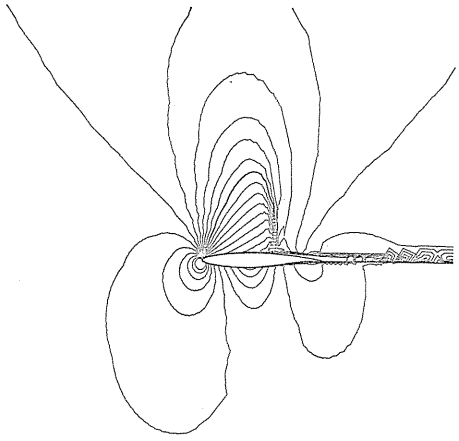

Fig. 3. The equi-Mach-number lines ($\Delta M=0.04$).

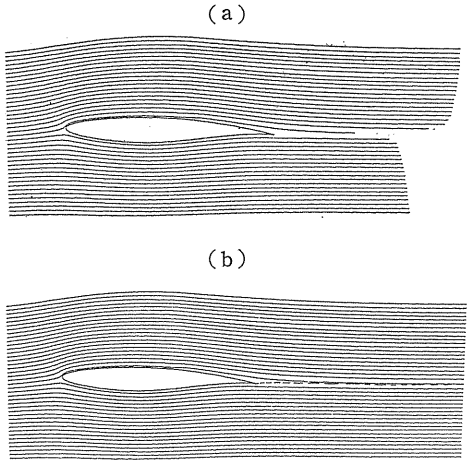

Fig. 4. Particle paths and wake.

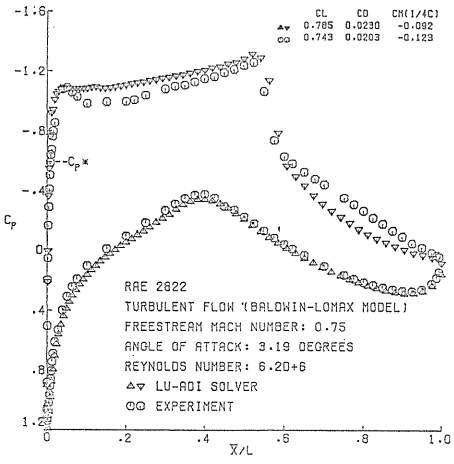

Fig. 5. Pressure distribution over the airfoil surface.

be estimated that the dashed line is approximately a streamline corresponding to the trailing edge.

Fig. 5 shows a comparison between calculated results and experimental values. The calculation of C_L, C_D (induced drag) and C_M does not include the effect of friction; they are close to the experimental values. Because we have not considered the effect of wind tunnel wall in the above calculation, the difference between both results may not be significant.

Appendix A

The flux Jacobian matrices $\hat{A}$ and $\hat{B}$ have real eigenvalues and a complete set of eigenvectors. The similarity transformations are

$$\hat{A}=T_\xi \Lambda_\xi T_\xi^{-1}, \quad \hat{B}=T_\eta \Lambda_\eta T_\eta^{-1}, \tag{A.1}$$

where

$$\Lambda_\xi=\begin{pmatrix}\hat{u} & & & \\ & \hat{u} & & \\ & & \hat{u}+a\sqrt{\tilde{\xi}_x^2+\tilde{\xi}_y^2} & \\ & & & \hat{u}-a\sqrt{\tilde{\xi}_x^2+\tilde{\xi}_y^2}\end{pmatrix}, \tag{A.2}$$

$$\Lambda_\eta=\begin{pmatrix}\hat{v} & & & \\ & \hat{v} & & \\ & & \hat{v}+a\sqrt{\eta_x^2+\eta_y^2} & \\ & & & \hat{v}-a\sqrt{\eta_x^2+\eta_y^2}\end{pmatrix}, \tag{A.3}$$

with

$$T_k=\begin{pmatrix}1 & 0 & \alpha & \alpha \\ u & \tilde{k}_y\rho & \alpha(u+\tilde{k}_x a) & \alpha(u-\tilde{k}_x a) \\ v & -\tilde{k}_x\rho & \alpha(v+\tilde{k}_y a) & \alpha(v-\tilde{k}_y a) \\ \dfrac{\phi^2}{\gamma-1} & \rho(\tilde{k}_y u-\tilde{k}_x v) & \alpha\left[\dfrac{\phi^2+a^2}{\gamma-1}+a\tilde{\theta}\right] & \alpha\left[\dfrac{\phi^2+a^2}{\gamma-1}-a\tilde{\theta}\right]\end{pmatrix}, \tag{A.4}$$

$$T_k^{-1}=\begin{pmatrix}(1-\phi^2/a^2) & (\gamma-1)u/a^2 & (\gamma-1)v/a^2 & -(\gamma-1)/a^2 \\ -(\tilde{k}_y u-\tilde{k}_x v)/\rho & \tilde{k}_y/\rho & -\tilde{k}_x/\rho & 0 \\ \beta(\phi^2-a\tilde{\theta}) & \beta[\tilde{k}_x a-(\gamma-1)u] & \beta[\tilde{k}_y a-(\gamma-1)v] & \beta(\gamma-1) \\ \beta(\phi^2+a\tilde{\theta}) & -\beta[\tilde{k}_x a+(\gamma-1)u] & -\beta[\tilde{k}_y a+(\gamma-1)v] & \beta(\gamma-1)\end{pmatrix}, \tag{A.5}$$

and $\alpha=\rho/(\sqrt{2}a)$, $\beta=1/(\sqrt{2}\rho a)$, $\phi^2=(\gamma-1)(u^2+v^2)/2$, $\tilde{\theta}=\tilde{k}_x u+\tilde{k}_y v$, and, for example, $\tilde{k}_x=k_x/\sqrt{k_x^2+k_y^2}$ ($k=\xi$ or η for $\hat{A}$ or $\hat{B}$).

The matrix $(T_\xi^{-1}T_\eta)^{-1}=T_\eta^{-1}T_\xi$ possesses a simple form, that is

$$T_\eta^{-1}T_\xi=\begin{pmatrix}1 & 0 & 0 & 0 \\ 0 & m_1 & \mu m_2 & -\mu m_2 \\ 0 & -\mu m_2 & \mu^2(1+m_1) & \mu^2(1-m_1) \\ 0 & \mu m_2 & \mu^2(1-m_1) & \mu^2(1+m_1)\end{pmatrix}, \tag{A.6}$$

where $m_1=(\tilde{\xi}_x\tilde{\eta}_x+\tilde{\xi}_y\tilde{\eta}_y)$, $m_2=(\tilde{\xi}_x\tilde{\eta}_y-\tilde{\xi}_y\tilde{\eta}_x)$ and $\mu=1/\sqrt{2}$. It is a function only of the metrics and not of the flow variables.

Appendix B

From the mass conservation, momentum conservation and sound speed equations

$$\frac{\partial \rho}{\partial t}+\frac{\partial(\rho u)}{\partial x}=0, \tag{B. 1}$$

$$\frac{\partial u}{\partial t}+u\frac{\partial u}{\partial x}+\frac{1}{\rho}\frac{\partial p}{\partial x}=0, \tag{B. 2}$$

$$a^2=\left(\frac{\partial p}{\partial \rho}\right)_s, \tag{B. 3}$$

we have

$$\frac{\partial u}{\partial t}\pm\frac{1}{\rho a}\frac{\partial p}{\partial t}+\left(\frac{\partial u}{\partial x}\pm\frac{1}{\rho a}\frac{\partial p}{\partial x}\right)(u\pm a)=0. \tag{B. 4}$$

Asssuming $J_\pm=u\pm\int\frac{dp}{\rho a}$, Eq. (B. 4) expresses that $J_\pm$ are invariants along characteristic lines $dx/dt=u\pm a$, respectively, called Riemann invariants. Using Eq. (B. 3) and the entropy condition

$$p/\rho^\gamma=c, \tag{B. 5}$$

we obtain

$$\int\frac{dp}{\rho a}=\int\frac{\sqrt{c\gamma\rho^{\gamma-1}}\,d\rho}{\rho}=\sqrt{c\gamma}\int\rho^{\frac{\gamma-3}{2}}d\rho=\sqrt{c\gamma}\,\frac{2}{\gamma-1}\rho^{\frac{\gamma-1}{2}}=\frac{2}{\gamma-1}a, \tag{B. 6}$$

and

$$J_\pm=u\pm\frac{2}{\gamma-1}a. \tag{B. 7}$$

References

1) Y. Y. Wang and T. Fujiwara; Numerical Analysis of Transonic Flow around a Two-Dimensional Airfoil by Solving Full Navier-Stokes Equations, Memoirs of the Faculty of Engineering, Nagoya University, Vol. 36, No. 2, pp. 138-178, 1984.
2) T. Fujiwara, Y. Y.Wang and Y. Ohmori; Turbulent Transonic Flow for NACA 0012/RAE 2822 Airfoils under Baldwin-Lomax Model, Memoirs of the Faculty of Engineering, Nagoya University, Vol. 37, No. 2, pp. 203-218, 1985.
3) T. J. Barth and J. L. Steger; A Fast Efficient Implicit Scheme for the Euler and Navier-Stokes Equations Using Matrix Reduction Techniques, Submitted to AIAA 23rd Aerospace Sciences Meeting, Reno, Nev. 1985.
4) T. H. Pulliam and J. L. Steger; Recent Improvements in Efficiency, Accuracy and Convergence for Implicit Approximate Factorization Algorithms, AIAA Paper 85-0360.

5) S. Obayashi, K. Matsushima, K. Fujii and K. Kuwahara; Improvements in Efficiency and Reliability for Navier-Stokes Computations Using the LU-ADI Factorization Algorithm, AIAA Paper 86-0338.
6) T. H. Pulliam; Artificial Dissipation Models for the Euler Equations, AIAA Paper 85-0438.
7) Y. Ohmori; Transonic Turbulent Flow around Two-Dimensional Airfoils, Proceedings of the Fifteenth International Symposium on Space Technology and Science, Tokyo, pp. 2185-2193, 1986.